Journal of Magnetism and Magnetic Materials 401 (2016) 1123–1129

Contents lists available at ScienceDirect

Journal of Magnetism and Magnetic Materials

journal homepage: www.elsevier.com/locate/jmmm

Current Perspectives

Three-dimensional atom probe analysis and magnetic properties of $Fe_{85}Cu_1Si_2B_8P_4$ melt spun ribbons

S. Jafari [a,b,*], A. Beitollahi [b], B. Eftekhari Yekta [b], T. Ohkubo [a], Viktoria Budinsky [c], Mie Marsilius [c], S. Mollazadeh [d], Giselher Herzer [c], K. Hono [a]

[a] Magnetic Materials Unit, National Institute for Materials Science, 1-2-1 Sengen, Tsukuba 305-0047, Japan
[b] Center of Excellence for Ceramics in Energy and Environment, School of Metallurgy and Materials Engineering, Iran University of Science and Technology (IUST), Narmak, Tehran 16846-13114, Iran
[c] Vacuumschmelze GmbH, D-63450 Hanau, Germany
[d] Department of Material Engineering, Faculty of Engineering, Ferdowsi University of Mashhad, Mashhad, Iran

ARTICLE INFO

Article history:
Received 11 July 2015
Received in revised form
15 September 2015
Accepted 27 October 2015
Available online 28 October 2015

Keywords:
Three-dimensional atom probe analysis
Magnetic properties
Nanocrystalline alloys
Microstructure
Melt spinning

ABSTRACT

The effect of phosphorous on the microstructure and magnetic properties of as-spun and flash annealed (389–535 °C for 7 s) $Fe_{85}Cu_1Si_2B_8P_4$ melt spun ribbons were investigated by three-dimensional atom probe (3DAP) and high resolution transmission electron microscopy (HRTEM) techniques. The formation of quasi-amorphous α-Fe clusters of 3–5 nm size in an amorphous matrix were detected by HRTEM, despite the high quenching rate applied by high wheel speed used. Flash annealing of the as-spun ribbons gave rise to the formation of nanocrystalline α-Fe (Si) phase in amorphous matrix containing Fe, Si, B and P elements as detected by 3DAP. Comparing 3DAP analysis of the samples annealed at 445 °C and 535 °C revealed that the concentration of P and B in amorphous matrix were increased for the latter. Further, it was shown that P hardly solidified into nanocrystalline phase and partitioned in amorphous phase alongside B atoms leading to the further stabilization of amorphous matrix as confirmed by 3DAP analysis. The highest magnitude of saturation magnetic induction ($B_s \sim 1.85$ T) and the lowest coercive field ($\sim$10–20 A/m) were obtained for the samples annealed above 445 °C, for which noticeable reduction of saturation magnetostriction (λ_s) were also detected.

© 2015 Elsevier B.V. All rights reserved.

1. Introduction

Nanocrystalline Fe-based soft magnetic alloys obtained by crystallizing melt-spun amorphous ribbons have attracted great attention due to their excellent soft magnetic properties such as low coercivity (H_c), high permeability (μ) and very low saturation magnetostriction (λ_S) [1–8]. Considerable attempts have been made to improve the magnetic properties of this group of soft magnetic materials to make them competitive with Si steels. This has led to the development of new alloys with the aim to obtain higher saturation magnetic induction (B_s) as well as low core loss giving rise to the increase of efficiency of electrical machines and higher energy saving. The Fe-based nanocrystalline alloys normally contains rather large amounts of glass making elements to attain an amorphous matrix in which nanocrystalline phase/s could be crystallized by appropriate subsequent heat treatment. The incorporation of large amounts of such non-magnetic elements in such alloy system causes remarkable decrease in B_s. The highest B_s (1.7 T) already reported for Fe-based nanocrystalline alloys is about 80% of that of Silicon steels [4,5,9–11]. The substitution of cobalt for iron in Fe-based nanocrystalline alloys has led to the increase of M_s (1.8 T) [12]. However, using cobalt in Fe-based soft magnetic materials normally increases both the cost and the magnitude of coercivity [3]. Recently Fe-based soft magnetic alloys containing phosphorous (Fe–Cu–Si–B–P) have been developed [13–22]. This alloy system brought some significant advantages. The high amount of iron in these alloys ($>$ 80 at%) resulted in increasing B_s up to 1.9 T which was almost comparable to that of electrical steels [13–15]. Furthermore, the simultaneous additions of phosphorous and copper led to the decrease of α-Fe grain sizes within the remaining ferromagnetic amorphous phase. Despite the valuable works which have been done to introduce the superior magnetic properties of these alloy systems [13,17,23,24] alongside comprehensive TEM studies [25–27], unfortunately, there are not much detailed studies on the microstructural analysis of Fe–Cu–Si–B–P soft magnetic alloys using 3DAP. Recently authors presented the detail microstructural analysis of

* Corresponding author at: Center of Excellence for Ceramics in Energy and Environment, School of Metallurgy and Materials Engineering, Iran University of Science and Technology (IUST), Narmak, Tehran 16846-13114, Iran.
E-mail address: sahar_jafari@iust.ac.ir (S. Jafari).

http://dx.doi.org/10.1016/j.jmmm.2015.10.106
0304-8853/© 2015 Elsevier B.V. All rights reserved.

the $Fe_{84.3}Si_4B_8P_3Cu_{0.7}$ melt spun ribbons and discussed on the effect of phosphorous on magnetic properties of the flash annealed ribbons based on 3DAP analysis [28]. 3DAP and HRTEM analyses of $Fe_{84.3}Cu_{0.7}Si_4B_8P_3$ revealed that boron and phosphorous were rejected from α-Fe (Si) phase and enriched in the residual amorphous phase resulting in further stabilization of amorphous matrix leading to improve the magnetic properties of the ribbons [28]. In the work presented here, attempt is made to study the as-spun and annealed nanocrystalline ribbons of $Fe_{85}Si_2B_8P_4Cu_1$ alloy using HRTEM and 3DAP with the aim to understand the phase evolution of the nanocrystalline phase/s of the as-spun and rapidly annealed ribbons. Further, structural/microstructural–magnetic properties correlations are also discussed.

2. Material and methods

$Fe_{85}Si_2B_8P_4Cu_1$ ingot was prepared by induction melting the mixture of Fe (> 99.99 wt%), Cu (> 99.99 wt%), Si (> 99.99 wt%) and master alloys of Fe_3P (> 99.9 wt%) and Fe–B (> 99.9 wt%) in an argon atmosphere. Amorphous ribbons of $Fe_{84.3}Si_4B_8P_3Cu_{0.7}$ composition (hereafter referred as P_4 as-spun alloy) with the thickness of ~18 μm and ~10 mm width were prepared by rapid quenching from the melt via melt spinning at 40 m/s wheel speed. Thermal analysis of as-spun ribbons was performed by differential scanning calorimeter (DSC) at a heating rate of 10 K/min. The as-spun ribbons were annealed under a tensile stress of 22 MPa along the ribbon axis. For this purpose the ribbons were continuously transported through a furnace with an approximately 10 cm long homogenous temperature zone kept under nitrogen atmosphere. The ribbons were guided in close contact to an annealing fixture made of stainless steel in order to ensure a good heat transfer. The annealing temperature, T_a, was measured by a thermocouple attached to the fixture in the center of the oven. The annealing speed was 1.6 m/min which corresponds to an annealing time of about 7 s at T_a with heating and cooling rates in the range of 100–200 K/s. The annealing explained above is called flash annealing. The studied annealed samples are presented by a code referring to the alloy composition (i.e. P_4) followed by their respective annealing temperatures. Inline recording of the a.c. (60 Hz) B–H loop after annealing was carried out for all of the heat-treated samples. Coercivity was determined either from the hysteresis loops or, in particular for high anisotropies, with a Förster Koerzimat 1.096 [29]. The saturation magnetostriction, λ_s, was measured by the small angle magnetization rotation (SAMR) method [30,31]. Microstructural studies were carried out with high-resolution transmission electron microscopy (HRTEM) using a FEI Tecnai G2 F30. Thin foil specimens for TEM observations were prepared by dimple grinding followed by ion milling using precision ion polishing system (PIPS) at cold stage. A locally built laser-assisted three-dimensional atom probe (LA3DAP) with CAMECA's fast delay line detector was used for atom probe analyses. A femto-second pulsed laser with a wave length of 343 nm was used to assist field evaporation of atoms [32]. Needle-like specimens for the 3DAP analyses were prepared by the micro-sampling technique using a focused ion beam, Hitachi FB-2100, and by the annular focused Ga ion beam using a Carl Zeiss Cross Beam 1540 EsB [33].

3. Results and discussion

3.1. Structural/microstructural analysis

Fig. 1 shows the XRD patterns of the as-spun and annealed samples. As can be realized from these patterns, only one broad peak around 2 $\theta = 45^\circ$ could be noticed for as-spun sample

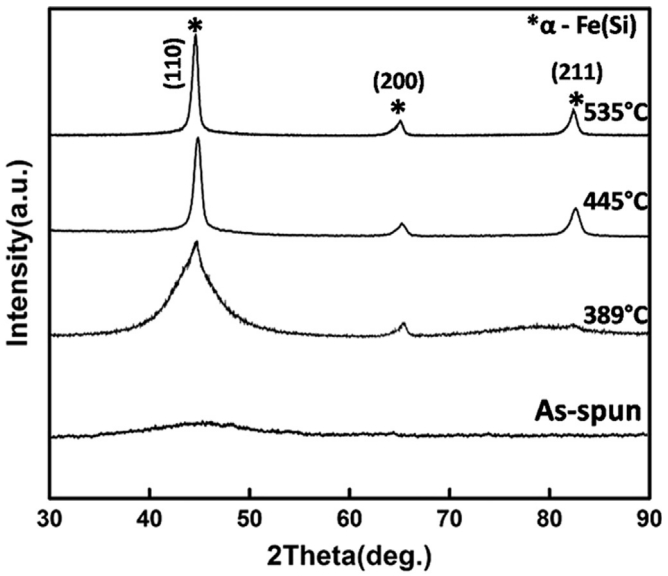

Fig. 1. XRD patterns of the as-spun and annealed $Fe_{85}Cu_1Si_2B_8P_4$ alloys.

indicating that this sample was amorphous, within the detection accuracy of XRD technique. This was also confirmed by our TEM results.

Fig. 2(a) demonstrates TEM micrograph of the as-spun sample along with the respective selected area electron diffraction (SAED) pattern. As can be realized from this figure, the classic feature of the amorphous materials in SAED (presence of halo diffraction rings) was noticed for the as-spun ribbons. However, the HRTEM micrograph (Fig. 2b) revealed the existence of very fine crystallites with the size in the range of about 3–5 nm randomly dispersed in amorphous matrix, suggesting the formation of a quasi-amorphous structure for as-spun ribbons. The lattice fringes of the observed crystallites (inset of Fig. 2(b)) corresponds to (110) plane of bcc α-Fe phase. The existence of primary crystals in the as-quenched state has also been reported in Fe–Cu–B and Fe–Cu–Si–B alloys [4,5,34,35]. Besides, most of previous studies on Fe–Cu–Si–B–P alloy systems containing Fe content of higher than 80 at% has also confirmed the formation quasi-amorphous structure [13,15,23]. The existence of primary crystals suggests that in the present alloy system, nanocrystallization has somewhat occurred by primary crystallization mode. Since the composition of primary crystals are different than that of the amorphous matrix, diffusion and partitioning of solute atoms are involved in this process. The microstructure obtained by this mode of crystallization is generally very fine because its grain growth is diffusion-controlled [36].

Fig. 3 also displays the DSC curve of P_4 as-spun alloy with two strong exothermic peaks of crystallizations at 378 °C and 522 °C. The first temperature (T_{x1}) was related to the primary crystallization of the nanocrystalline phase, i.e. α-Fe (Si) soft ferromagnetic phase. The second one (T_{x2}) was attributed to the crystallization of Iron boride phase(s) from the residual amorphous phase [3]. It was already reported that the simultaneous addition of phosphorous and copper rose the temperature interval (ΔT) between T_{x1} and T_{x2} [13,14,17,18]. T_{x1} can be considered as a parameter to determine the thermal stability of the amorphous phase in as-spun state and T_{x2}, as a parameter to determine the thermal stability of the remaining amorphous phase above T_{x1} [37]. According to previous studies [17], T_{x1} decreased with phosphorous addition. It is well known that the crystallization of Iron rich phases is initiated by Cu clusterization [36]. Since the mixing enthalpy (ΔH_{mix}) of Cu and P is negative [38] one could expect the possible formation of increased density of nucleation sites which

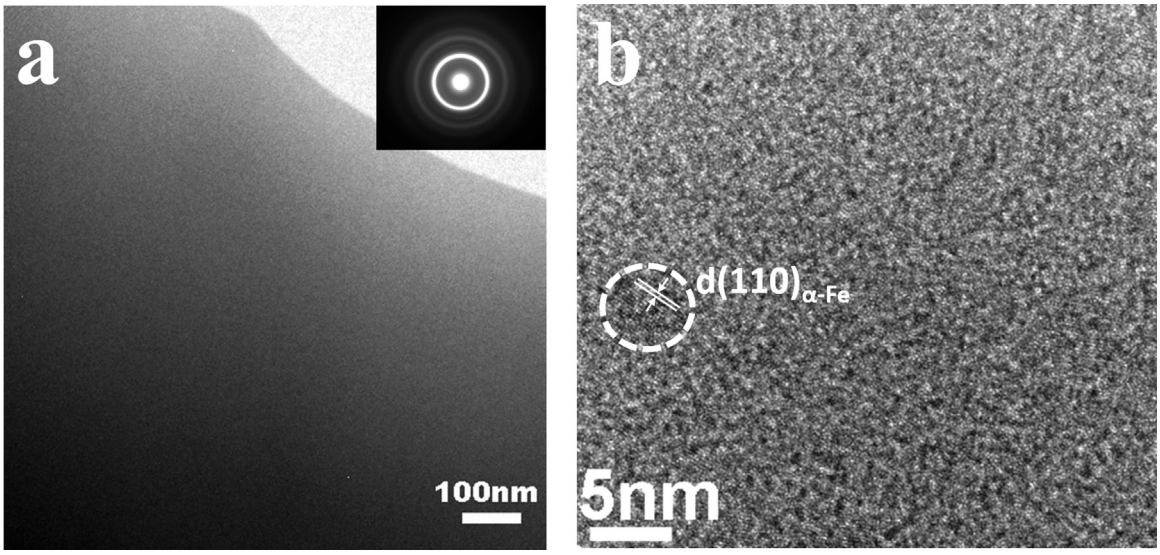

Fig. 2. TEM micrographs of the as-spun $Fe_{85}Cu_1Si_2B_8P_4$ ribbon. (a) Bright field image and the corresponding SAED pattern. (b) High resolution micrograph showing lattice fringes in broken line area.

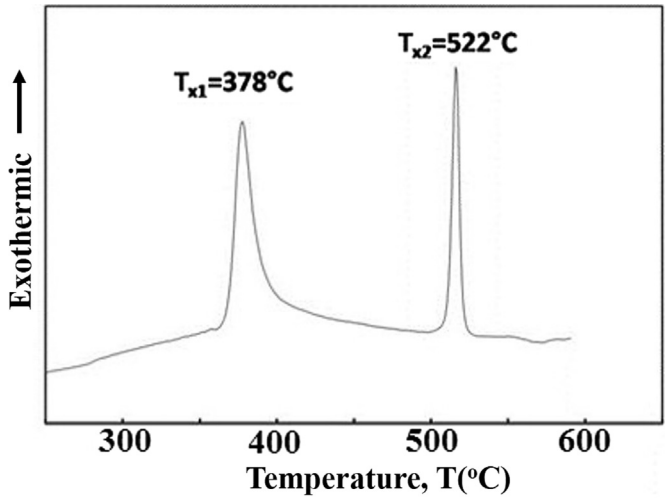

Fig. 3. DSC curve of $Fe_{85}Cu_1Si_2B_8P_4$ as-spun ribbons.

could eventually affect nanocrystallization of the prepared ribbons [36,38].

The existence of rather wide ΔT is in favor of nanocrystallization of α-Fe (Si) phase without initiating boride phase/s formation which deteriorates soft magnetic properties of the annealed ribbons [17]. Fig. 4(a–e) shows the 3DAP elemental maps of the as-spun sample within an analyzed volume of $160 \times 36 \times 5.5$ nm^3. The actual alloy composition obtained for as-spun sample is as follows: Fe=85 at%, Si=2.19 at%, P=5.14 at%, B=6.71 at%, Cu=0.96 at%. The obtained concentrations have about 2% error from nominal value which is within the experimental error of atom probe. Moreover, as can be realized from Fig. 4(a–e), all of the elements seem to be distributed uniformly in the specimen. As no compositional change occurred in the formation of the very fine iron clusters and the only change was structural, the very small heterogeneities could not be detected in 3DAP elemental map of Iron.

Fig. 5(a–e) shows the 3DAP elemental map of iron, boron, phosphorous, silicon and copper at 389 °C (sample P_4-389). The elemental map of copper analyzed by IVAS software clearly demonstrated that Cu-enriched clusters were dispersed through the specimen at the onset of crystallization. Fig. 6(a) shows the sliced

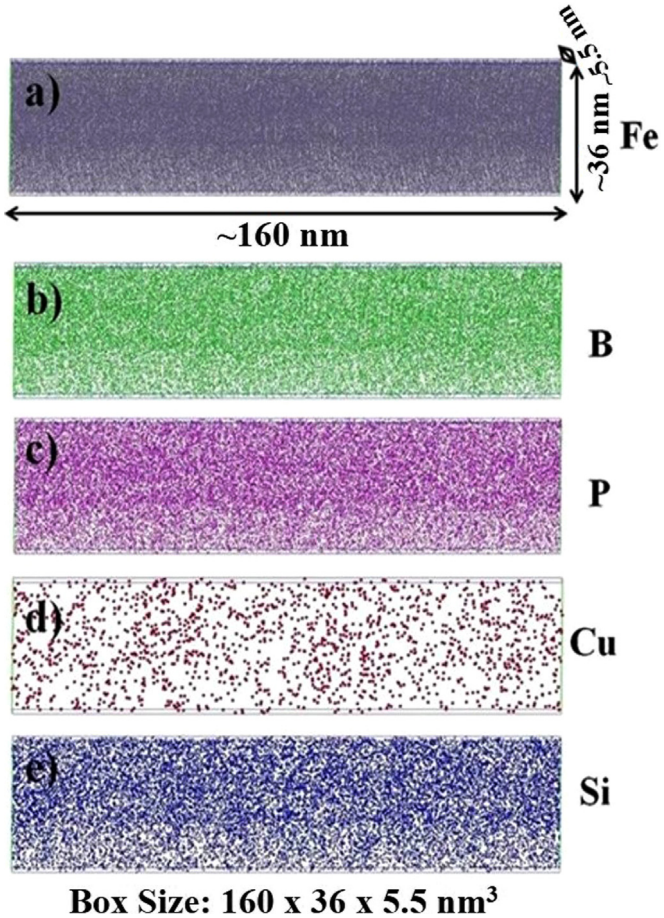

Fig. 4. 3DAP elemental maps ($160 \times 36 \times 5.5$ nm^3) of (a) Fe, (b) B, (c) P, (d) Cu and (e) Si atoms for as-spun $Fe_{85}Cu_1Si_2B_8P_4$.

elemental map of copper in a volume of $130 \times 23.5 \times 7.5$ nm^3. The inset illustrates a sliced elemental map of copper around one copper enriched cluster in a volume of $15 \times 3 \times 3$ nm^3. The integrated concentration depth profiles of iron, boron, phosphorous and copper atoms corresponding to this sliced volume are shown in Fig. 6(b). The concentration of each atom around the

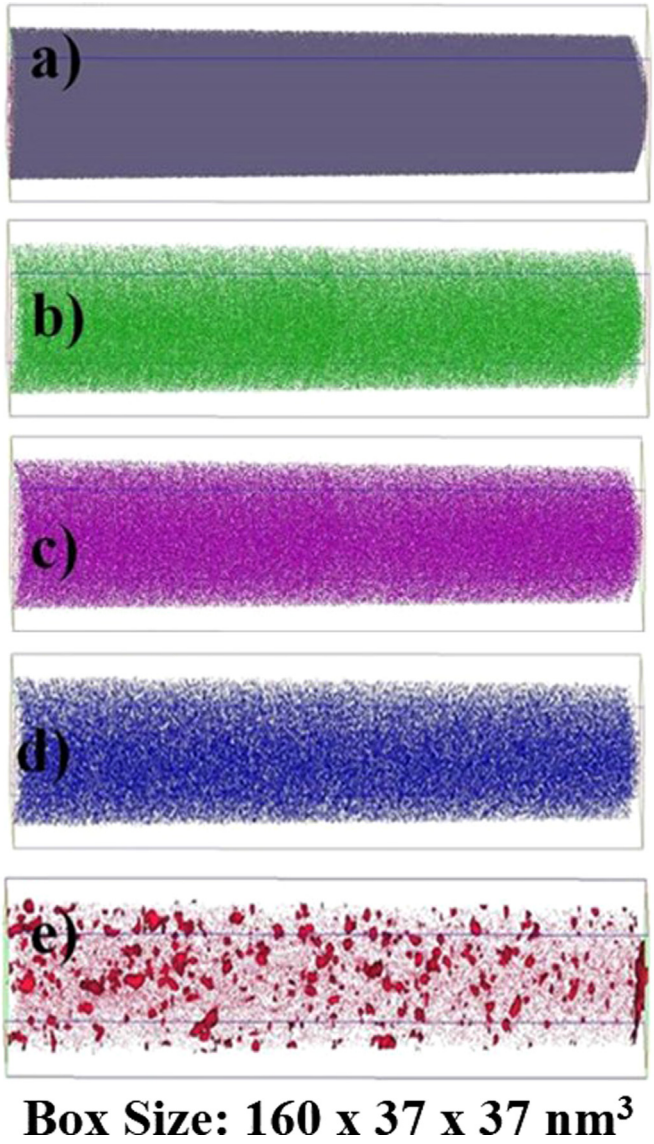

Fig. 5. (a) 3DAP elemental map ($160 \times 37 \times 37$ nm^3) of (a) Fe, (b) B, (c) P, (d) Cu and (e) Si atoms for $Fe_{85}Cu_1Si_2B_8P_4$ alloy flash annealed at 389 °C for 7 s (P_4-389 sample).

copper cluster, calculated from the slope of the ladder diagrams (insets of Fig. 6(b)) showed that except for the copper, there was not any appreciable concentration change for the other elements around copper clusters. Besides, the absence of nano grains in the atomic maps proved that the crystallization of α-Fe (Si) nanocrystals did not occur yet at the onset of crystallization possibly due to the rather short soaking time (7 s) applied for this sample. For P_4-389 sample, homogeneous distribution of copper clusters was noticeable (Fig. 5(e)) indicating that clustering of copper had occurred. This was not noticed in the case of as-spun ribbons (Fig. 4(d)).

In multi component alloy systems if an element with a large positive enthalpy of mixings with the main constituent element is added to an alloy, phase decomposition of that particular element can occur in glassy state [36]. This was observed in FINEMET alloys [39] for copper element which has large positive enthalpy of mixing with iron [36,38]. One could suggest that this has also happened in the present alloy system in which copper atoms have formed clusters in the amorphous state.

The concentration of Cu atoms in copper clusters has been estimated to be approximately 1.4 at% in P_4-389 sample (Fig. 6(b)),

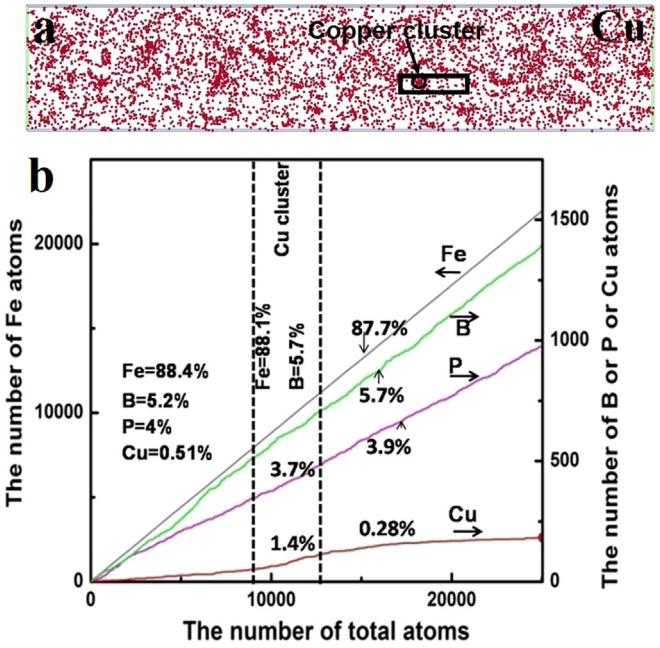

Fig. 6. (a) 3DAP elemental map ($130 \times 23.5 \times 7.5$ nm^3) of Cu atoms for P_4-389 sample. (b) Integrated concentration depth profiles (ladder diagrams) from sliced volume shown in (a) containing Cu cluster. The concentrations of each atom calculated from the slope of ladder diagram are shown in (b).

which is very low compared to that of the samples annealed at higher temperatures as shown later. This has been also reported by others for FINEMET nanocrystalline alloys [36] as well. The copper clusters serve as heterogeneous nucleation sites for further crystallization of α-Fe nanocrystals. It is worth to mention that primary crystals assist nucleation by providing heterogeneous nucleation sites as well.

Fig. 7(a–e) shows the sliced 3DAP elemental mappings of iron, boron, phosphorous, copper and silicon atoms for the P_4-445 sample. As can be seen in Fig. 7(a), the iron enriched regions representing α-Fe (Si) crystals were clearly observed in iron map of this sample. The elemental maps of boron and phosphorous atoms indicated that boron and phosphorous were rejected from α-Fe (Si) phase and enriched in the residual amorphous phase (Fig. 7(b and c)). Copper clusters were distributed over the specimen homogenously to induce nucleation of nanocrystals (Fig. 7(d)).

Fig. 7(f) shows the integrated concentration depth profiles of iron, boron, phosphorous and copper atoms for the selected area (shown in Fig. 7(d)) around copper enriched clusters. Based on 3DAP analysis (Fig. 7(f)) copper clusters for the P_4-445 sample were in direct contact with α-Fe (Si) grains suggesting that copper clusters acted as heterogeneous nucleation sites for the α-Fe (Si) phase crystallization. The concentration of copper for the P_4-445 sample was higher than that of P_4-389 sample (i.e. 1.8–1.4 at%). On the other hand, the enrichment of remaining amorphous phase by rejected atoms (B and P) results in the stabilization of amorphous phase. The stabilized amorphous phase suppresses the grain growth. As shown before by authors [24], for $Fe_{84.3}Si_4B_8P_3Cu_{0.7}$ alloys, in case of the annealed samples, boron and phosphorous together partitioned in the amorphous phase. The existence of primary crystals in as-spun samples and copper clusters could both possibly help nucleation by providing suitable sites initiating the formation of increased number of nanocrystalline grains. This would result to increase partitioning of P and B leading to the further stabilization of amorphous matrix. This is expected to hinder the grain growth [17].

It is already shown that, increasing the annealing temperature decreases the number density of copper clusters while rising the

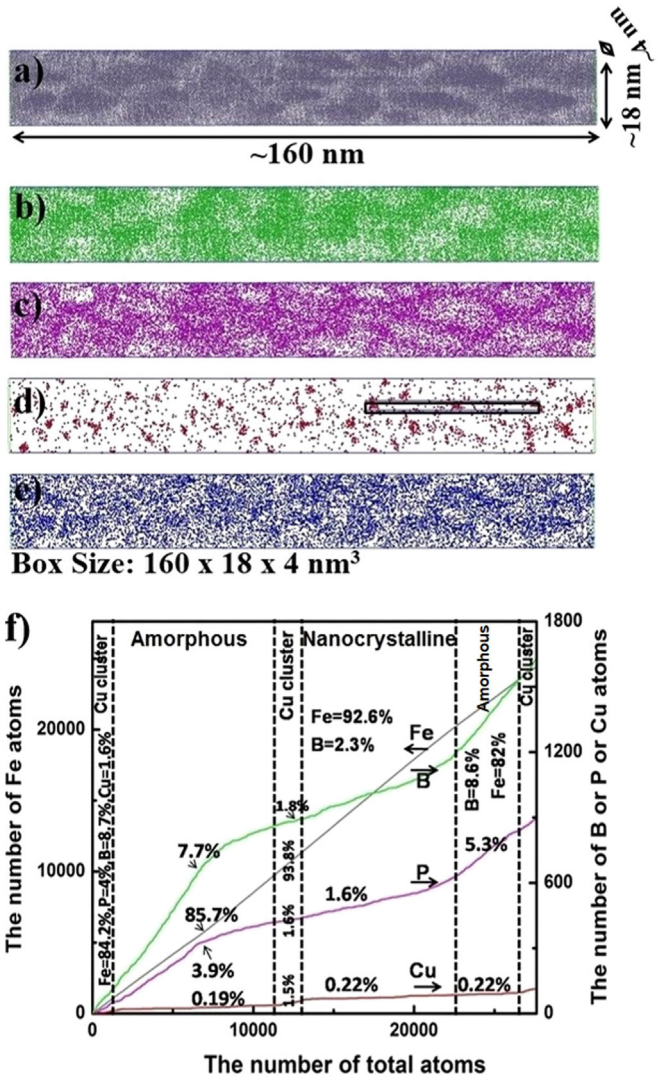

Fig. 7. 3DAP elemental map ($160 \times 18 \times 4\ nm^3$) of (a) Fe, (b) B, (c) P, (d) Cu and (e) Si atoms obtained for P_4-445 sample. (f) Integrated concentration depth profiles (ladder diagrams) from selected area in (d). The concentrations of each atom calculated from the slope of ladder diagram are shown in (f).

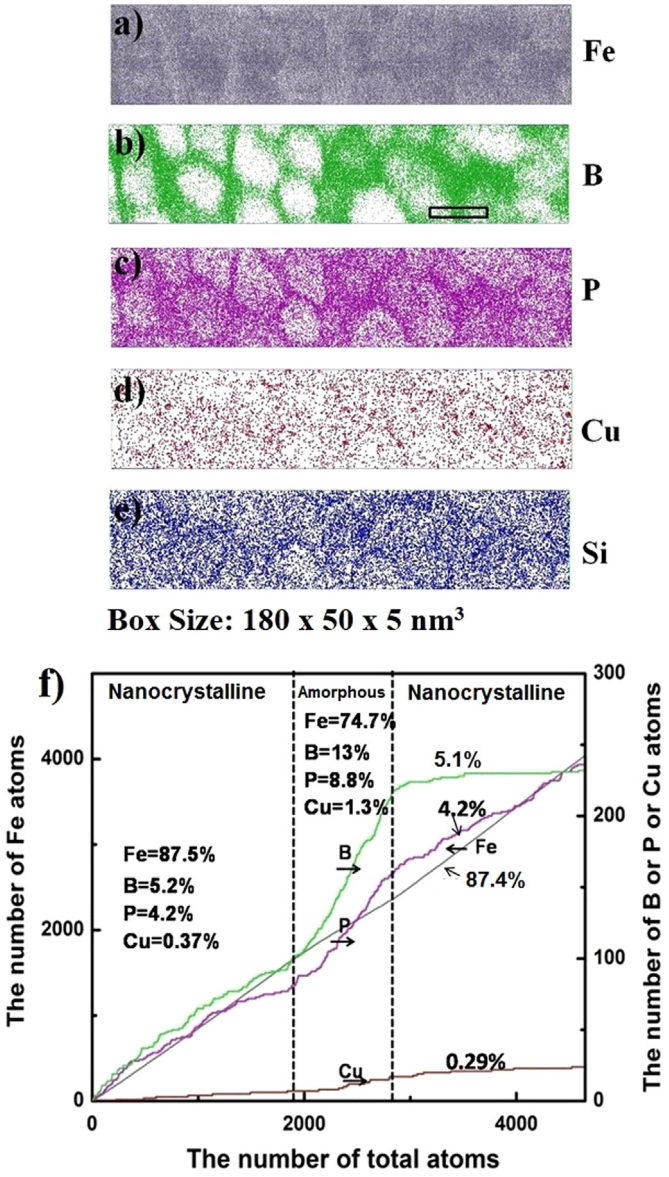

Fig. 8. 3DAP elemental map ($180 \times 50 \times 5\ nm^3$) of (a) Fe, (b) B, (c) P, (d) Cu and (e) Si atoms obtained for P_4-535 sample. (f) Integrated concentration depth profiles (ladder diagrams) from selected area in (b). The concentrations of each atom calculated from the slope of ladder diagram are shown in (f).

concentration of copper in enriched copper clusters [36].

Fig. 8(a–d) demonstrates the elemental mappings of iron, boron, phosphorous, silicon and copper for P_4-535 sample. Fig. 8 (f) shows the integrated concentration depth profiles of iron, boron, phosphorous and copper atoms for the selected area related to one grain boundary and two grains. Comparison the elemental concentrations of both nanocrystalline (α-Fe (Si)) and amorphous phases for the P_4-445 and P_4-535 samples (Figs. 7(f) and 8(f)) show that increasing the annealing temeperature led to the rise of phosphorous and boron contents partitioning in remaining amorphous phase (i.e. ~7.7 at% B and ~5.3 at% P in the amorphous matrix of P_4-445 sample to ~13 at% B and ~8.8 at% P in the amorphous matrix of P_4-535 sample).

3.2. Magnetic properties

Fig. 9 demonstrates B–H loops of various samples prepared in this work. As can be realized from this figure, the saturation magnetic induction increases from about $B_s = 1.5$ T in the amorphous state up to the highest magnitude of $B_s = 1.85$ T measured at a maximum field of ~3500 A/M for the samples annealed above 445 °C for which higher degree of crystallinity was detected by XRD technique. For magnetic nanocomposites alloys, one should consider that the M_S, and hence B_s, depends on the crystalline volume fraction (x) through the proportion of the different phases contributing to the total magnetization of the sample by considering that [40]:

$$M_s = M_{am}(1 - x) + M_{cr}(x) \quad (1)$$

where, M_{am} and M_{cr} refer to the saturation magnetization of the amorphous and crystalline phases, respectively.

Further, as can be depicted from Fig. 10 in general, the higher was the applied annealing temperature, the lower were the coercivities of the samples.

Fig. 10 displays the variation of coercivity (H_c) as well as saturation magnetostriction (λ_s) versus annealing temperature (T_a). The observed sharp decline of H_c values after the onset of crystallization is mainly due to the simultaneous decrease of magnetostriction and magnetocrystalline anisotropies [40]. Magnetostriction anisotropy is established by the alloy composition, which determines the magnetostriction constant and stress field which

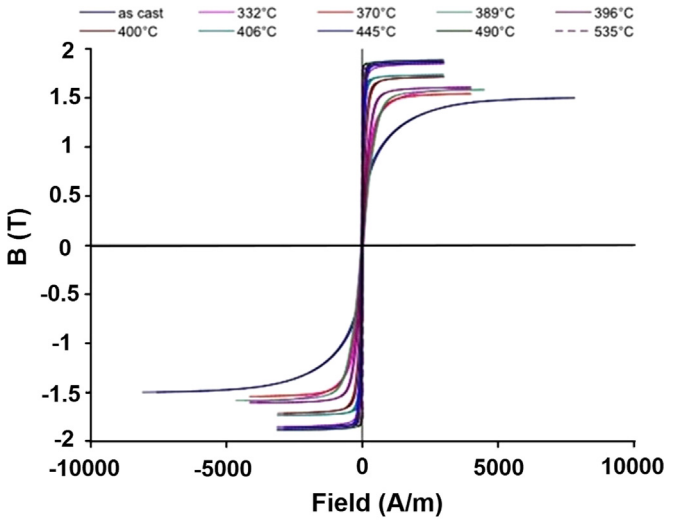

Fig. 9. The magnetization curves of as-spun and annealed $Fe_{85}Cu_1Si_2B_8P_4$ ribbons measured by VSM.

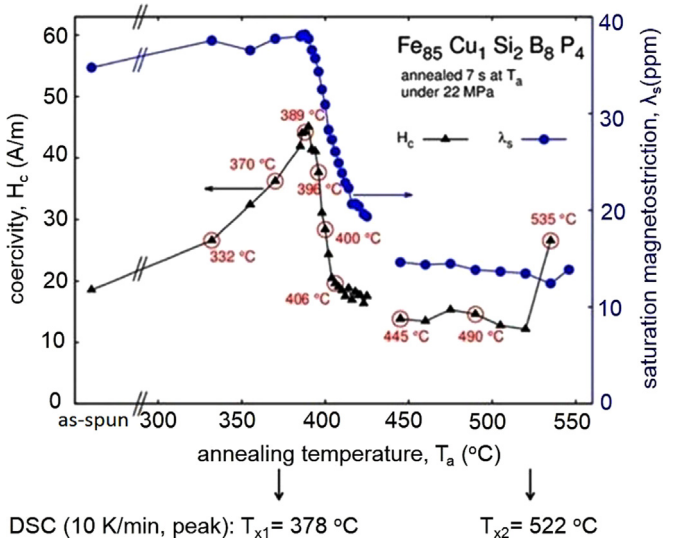

Fig.10. Annealing temperature dependence of H_c and λ_s for $Fe_{85}Cu_1Si_2B_8P_4$ alloys.

results from the fabrication process. The positive magnetostriction of the residual amorphous phase is balanced with the negative magnetostriction of nanocrystalline α-Fe (Si) phase with the negative magnetostriction. Based on the random anisotropy model developed by Herzer [2], it is known that the effective anisotropy contribution of the small randomly oriented α-Fe (Si) grains is reduced by exchange interaction. The critical scale where the exchange energy balance the anisotropy energy is $L_o=(A/K_1)^{1/2}$, where L_o is the exchange-correlation length, A is the exchange stiffness constant and K_1 is the magnetocrystalline anisotropy. L_o is about 35 nm for the bcc Fe–Si (20 at%) which is of the order of domain wall width. For $D \approx L_o/3$, i.e., grain sizes of the order of 10–15 nm, the magnetization will not follow the easy axis of the individual grains, but increasingly is forced to align parallel by exchange interaction. Consequently, the local anisotropies are averaged out over an increasing number of grains so that the effective anisotropy constant K_{eff} scales down as:

$$K_{eff} \approx KD^{3/2} \approx \left(\frac{K_{eff}}{A}\right)^{3/2} \approx \left(\frac{K^4D^6}{A^3}\right) \quad (2)$$

where K is the magnetocrystalline anisotropy constant of any grain and the D is the average grain size. Since H_c can be considered as proportional to the effective anisotropy, one can predict a similar variation of H_c with average grain size, D. The excellent soft magnetic properties obtained for the P_4-445 sample prepared here are attributed to the sharp decline of both the magnetocrystalline and magnetostriction anisotropies. However, the observed rise of H_c and λ_s for the samples heat-treated above 530 °C could be possibly related to the formation of borides in the system as the annealing temperature was very close to T_{x2} (522 °C).

4. Conclusions

In this work, microstructural and magnetic properties study of as-spun and flash annealed ribbons of $Fe_{85}Si_2B_8P_4Cu_1$ alloys were carried out. In this respect, the following conclusions were obtained:

1. For the as-spun sample, the existence of small clusters (~3–5 nm) of α-Fe phase could be detected within amorphous matrix based on the HRTEM analysis suggesting the existence of quasi-amorphous structure, despite the high speed wheel used during rapid quenching.
2. In the present alloy system studied here, boron and phosphorous together partitioned in remaining amorphous phase which led to the grain growth hindrance.
3. Increasing the annealing temperature led to the rise of phosphorous and boron contents partitioning in remaining amorphous phase.
4. The highest magnitude of B_S ($\sim$1.85 T) was obtained for the samples annealed above 445 °C for which higher degree of crystallinity was noticed.
5. The sharp decline of H_c was observed for the samples annealed above 445 °C due to the sharp decrease of magnetostriction and magnetocrystalline anisotropies.

Acknowledgments

S.J. acknowledges National Institute for Materials Science (NIMS), Japan for the provision of the NIMS Junior Research Assistantship for her Ph.D. research.

References

[1] G. Herzer, Grain size dependence of coercivity and permeability in nanocrystalline ferromagnets, IEEE Trans. Magn. 26 (1990) 1397–1402.
[2] G. Herzer, Grain structure and magnetism of nanocrystalline ferromagnets, IEEE Trans. Magn. 25 (1989) 3327–3329.
[3] M.E. McHenry, M.A. Willard, D.E. Laughlin, Amorphous and nanocrystalline materials for applications as soft magnets, Prog. Mater. Sci. 44 (1999) 291–433.
[4] M. Ohta, Y. Yoshizawa, Magnetic properties of nanocrystalline $Fe_{82.65}Cu_{1.35}SixB_{16-x}$ alloys (x=0–7), Appl. Phys. Lett. 91 (2007) 062517–062513.
[5] Motoki Ohta, Y. Yoshizawa, New high-B_s Fe-based nanocrystalline soft magnetic alloys, Jpn. J. Appl. Phys. 46 (2007) L477–L479.
[6] G. Herzer, Modern soft magnets: amorphous and nanocrystalline materials, Acta Mater. 61 (2013) 718–734.
[7] F. Shahri, A. Beitollahi, Effect of super-heat treatment and quenching wheel speed on the structure and magnetic properties of Fe–Si–Nb–Cu–B–Al–Ge melt spun ribbons, J. Non-Cryst. Solids 354 (2008) 1487–1493.
[8] F. Shahri, A. Beitollahi, S.G. Shabestari, M. Ghanaatshoar, M.M. Tehranchi, S. M. Mohseni, S.E. Roozmeh, N. Wanderka, F. Fiorillo, Structural characterization and magnetoimpedance effect in amorphous and nanocrystalline AlGe-substituted FeSiBNbCu ribbons, J. Magn. Magn. Mater. 312 (2007) 35–42.
[9] G.Y. Chin, J.H. Wernick, Soft magnetic metallic materials, in: E.P. Wohlfarth (Ed.), Handbook of Ferromagnetic Materials, Elsevier, The Netherlands, 1980, pp. 55–188.
[10] Y. Yoshizawa, S. Oguma, K. Yamauchi, New Fe-based soft magnetic alloys composed of ultrafine grain structure, J. Appl. Phys. 64 (1988) 6044–6046.

[11] Y. Ogawa, M. Naoe, Y. Yoshizawa, R. Hasegawa, Magnetic properties of high Fe-based amorphous material, J. Magn. Magn. Mater. 304 (2006) e675–e677.
[12] J.A. Vaccari, Des. Eng. 52 (1981).
[13] A. Makino, H. Men, T. Kubota, K. Yubuta, A. Inoue, New excellent soft magnetic FeSiBPCu nanocrystallized alloys with high B_s of 1.9 T From nanohetero-amorphous phase, IEEE Trans. Magn. 45 (2009) 4302–4305.
[14] A. Makino, H. Men, T. Kubota, K. Yubuta, A. Inoue, New Fe-metalloids based nanocrystalline alloys with high B_s of 1.9 T and excellent magnetic softness, J. Appl. Phys. 105 (2009) 07A308–303.
[15] Akihiro Makino, He Men, Takeshi Kubota, Kunio Yubuta, A. Inoue, FeSiBPCu nanocrystalline soft magnetic alloys with high B_s of 1.9 T produced by crystallizing hetero-amorphous phase, Mater. Trans. 50 (2009) 204–209.
[16] A. Makino, H. Men, K. Yubuta, T. Kubota, Soft magnetic FeSiBPCu hetero-amorphous alloys with high Fe content, J. Appl. Phys. 105 (2009) 013922–013924.
[17] A.D. Wang, H. Men, B.L. Shen, G.Q. Xie, A. Makino, A. Inoue, Effect of P on crystallization behavior and soft-magnetic properties of $Fe_{83.3}Si_4Cu_{0.7}B_{12-x}P_x$ nanocrystalline soft-magnetic alloys, Thin Solid Films 519 (2011) 8283–8286.
[18] T. Kubota, A. Makino, A. Inoue, Low core loss of $Fe_{85}Si_2B_8P_4Cu_1$ nanocrystalline alloys with high B_s and B800, J. Alloy. Compd. 509 (Supplement 1) (2011) S416–S419.
[19] A. Makino, T. Kubota, K. Yubuta, A. Inoue, A. Urata, H. Matsumoto, S. Yoshida, Low core losses and magnetic properties of $Fe_{85-86}Si_{1-2}B_8P_4Cu_1$ nanocrystalline alloys with high B for power applications (invited), J. Appl. Phys. 109 (2011) 07A302–305.
[20] F. Kong, H. Men, T. Liu, B. Shen, Effect of P to B concentration ratio on soft magnetic properties in FeSiBPCu nanocrystalline alloys, J. Appl. Phys. 111 (2012) 07A311–313.
[21] Z. Zhang, P. Sharma, A. Makino, Role of Si in high B_s and low core-loss $Fe_{85.2}B_{10-X}P_4Cu_{0.8}Si_X$ nano-crystalline alloys, J. Appl. Phys. 112 (2012) 103902–103908.
[22] A. Urata, M. Yamaki, K. Satake, H. Matsumoto, A. Makino, Magnetic properties and structure of $Fe_{83.3-85.8}B_{7.0-4.5}P_9Cu_{0.7}$ nanocrystalline alloys, J. Appl. Phys. 113 (2013) 17A311–313.
[23] Men He, Liying Cui, Takeshi Kubota, Kunio Yubuta, A. Makino, A. Inoue, Fe-rich soft magnetic FeSiBPCu hetero-amorphous alloys with high saturation magnetization, Mater. Trans. 50 (2009) 1330–1333.
[24] Z. Akase, S. Aizawa, D. Shindo, P. Sharma, A. Makino, In-situ Lorentz microscopy of Fe85Si2B8P4Cu1 nanocrystalline soft magnetic alloys, J. Magn. Magn. Mater. 375 (2015) 10–14.
[25] K. Sato, K. Takenaka, A. Makino, Y. Hirotsu, Direct imaging of structural heterogeneity of the melt-spun $Fe_{85.2}Si_2B_8P_4Cu_{0.8}$ alloy, AIP Adv. 5 (2015) 067166.
[26] A. Makino, Nanocrystalline soft magnetic Fe–Si–B–P–Cu alloys with high B of 1.8–1.9 T contributable to energy saving, Magn. IEEE Trans. 48 (2012) 1331–1335.
[27] P. Sharma, X. Zhang, Y. Zhang, A. Makino, Competition driven nanocrystallization in high B_s and low coreloss Fe–Si–B–P–Cu soft magnetic alloys, Scr. Mater. 95 (2015) 3–6.
[28] S. Jafari, A. Beitollahi, B. Eftekhari, T. Yekta, V. Ohkubo, M. Budinsky, G. Marsilius, K. Herzer, Hono Atom probe analysis and magnetic properties of nanocrystalline $Fe_{84.3}Si_4B_8P_3Cu_{0.7}$ 2015, in preparation.
[29] ⟨http://www.foerstergroup.com/KOERZIMAT-CS-coercivity-field-strenght.157.0.html⟩.
[30] K. Narita, J. Yamasaki, H. Fukunaga, Measurement of saturation magnetostriction of a thin amorphous ribbon by means of small-angle magnetization rotation, IEEE Trans. Magn. 16 (1980) 435–439.
[31] G. Herzer, S. Flohrer, C. Polak, Effect of stress annealing on the saturation magnetostriction of nanocrystalline $Fe_{73.5}Cu_1Nb_3Si_{15.5}B_7$, IEEE Trans. Magn. 46 (2010) 341–344.
[32] K. Hono, T. Ohkubo, Y.M. Chen, M. Kodzuka, K. Oh-ishi, H. Sepehri-Amin, F. Li, T. Kinno, S. Tomiya, Y. Kanitani, Broadening the applications of the atom probe technique by ultraviolet femtosecond laser, Ultramicroscopy 111 (2011) 576–583.
[33] M. Kodzuka, T. Ohkubo, K. Hono, F. Matsukura, H. Ohno, 3DAP analysis of (Ga, Mn)As diluted magnetic semiconductor thin film, Ultramicroscopy 109 (2009) 644–648.
[34] M. Ohta, Y. Yoshizawa, Cu addition effect on soft magnetic properties in Fe–Si–B alloy system, J. Appl. Phys. 103 (2008) E722–E723.
[35] Motoki Ohta, Y. Yoshizawa, Improvement of soft magnetic properties in $(Fe_{0.85}B_{0.15})_{100-x}Cu_x$ melt-spun alloys, Mater. Trans. 48 (2007) 2378–2380.
[36] K. Hono, Nanoscale microstructural analysis of metallic materials by atom probe field ion microscopy, Prog. Mater. Sci. 47 (2002) 621–729.
[37] T. Bitoh, A. Makino, A. Inoue, The effect of grain-size distribution on coercivity in nanocrystalline soft magnetic alloys, J. Magn. Magn. Mater. 272–276 (2) (2004) 1445–1446.
[38] A. Makino, M. Bingo, T. Bitoh, K. Yubuta, A. Inoue, Improvement of soft magnetic properties by simultaneous addition of P and Cu for nanocrystalline FeNbB alloys, J. Appl. Phys. 101 (2007) 09N117–113.
[39] K. Hono, D.H. Ping, M. Ohnuma, H. Onodera, Cu clustering and Si partitioning in the early crystallization stage of an $Fe_{73.5}Si_{13.5}B_9Nb_3Cu_1$ amorphous alloy, Acta Mater. 47 (1999) 997–1006.
[40] F. Shahri, A. Beitollahi, S.G. Shabestari, S. Kamali, Effects of heat treatment on the structure and magnetic properties of Al–Ge added $Fe_{73.5-x}Si_{13.5}B_9Nb_3Cu$ alloys, Phys. Rev. B 76 (2007) 024434.